Trends in Physical Chemistry
Vol. 22, 2022

Original Article

Electrokinetic flow and electric conduction of a salt-free solution in a charged slit

Yong J. Lin and Huan J. Keh*

Department of Chemical Engineering, National Taiwan University, Taipei 10617, Taiwan.

ABSTRACT

The electrokinetic flow and attended electric conduction of a salt-free fluid, which contains counterions only, in a narrow slit channel subjected to a pressure gradient and an electric field were analytically investigated. The surface charge densities of the two plane walls of the slit are uniform but can be unequal. The electric potential and fluid velocity profiles were determined by solving the exact and linearized Poisson-Boltzmann equations and modified Navier-Stokes equation, respectively. Explicit formulas were obtained for the electroosmotic velocity and electric conductivity as functions of a dimensionless surface charge density and the ratio of surface charge densities of the slit walls. The relative surface potentials, average electroosmotic velocity, and average electric conductivity grow monotonically with an increase in the dimensionless surface charge density (or ratio of the half thickness of the slit to the Debye screening length) for a given value of the surface charge density ratio. But, when the surface charge density is high, the growths of the relative surface potentials and average electroosmotic velocity with its increase are suppressed noticeably owing to the effect of counterion condensation. For a salt-free solution in a planar slit with two equally charged walls, its relative surface potential and average electroosmotic velocity are greater but its average electric conductivity is smaller than the corresponding results in a circular tube provided that the thickness of the slit equals the diameter of the tube.

*Corresponding author: huan@ntu.edu.tw

KEYWORDS: electroosmotic velocity, electric conductivity, salt-free fluid, slit microchannel and nanochannel, arbitrary surface charge densities.

1. Introduction

An ionic solution bounded by a charged solid surface makes up an electric double layer along their interface, where the diffuse ions have a net charge opposite in sign but equal in magnitude to that of the surface. When a charged microchannel or nanochannel filled with an ionic solution is subjected to an imposed electric field and/or pressure gradient that interact with the double layer, electrokinetic flows, such as electroosmosis, take place [1-6]. In addition to their fundamental interests in many scientific realms, electrokinetic flows have wide applications in the transport, separation, manipulation, mixing, and energy conversion of fluids in various practical systems (e.g., microfluidic and nanofluidic devices) [7-10].

The electrokinetic flow of a salt-free solution, containing no added electrolyte but solely counterions produced by a dissociation reaction occurring at a boundary, differs from that of a salt-containing solution [11-17]. When the charge density is high at the boundary, the counterions in the solution without added salt will be condensed remarkably in the double layer, known as the counterion condensation. Qiao and Aluru [18] investigated the electroosmosis of a salt-free solution in charged slit nanochannels and found that the fluid continuum theory is applicable for the case of channel widths of several nanometers. Ohshima [19] used a unit cell model to study the transverse

electroosmosis of salt-free solutions in a highly porous, fibrous matrix of parallel soft circular cylinders and disclosed that the electroosmotic mobility does not depend on the surface charge density, if it is higher than a critical value, due to the effect of counterion condensation. Chang *et al*. [20] examined the electroosmosis of some salt-free solutions in narrow circular channels theoretically and experimentally in the absence of the Debye screening effect and showed that the electroosmotic velocity grows with the channel radius. Chang [21-23] analyzed the transient electroosmosis of a salt-free solution in circular and slit microchannels and demonstrated that, due to the effect of counterion condensation, the rate of growth in the electroosmotic mobility with an increase in the surface charge density is substantially suppressed. Bandopadhyay and Chakraborty [24] theoretically studied the electroosmosis of counterion-only solutions in slit nanochannels and showed that the electroosmotic mobility is an increasing function of the surface charge density and ionic size. Recently, the axial electrokinetic flow and electric conduction of salt-free solutions in a fibrous porous matrix [25] and a circular tube [26] have been analyzed, and the results revealed that, when the porosity and surface charge density are high, the increases of the surface potential and electroosmotic mobility with the surface charge density are considerably suppressed owing to the counterion condensation effect.

In this article, the electrokinetic flow of salt-free solutions in a planar slit microchannel or nanochannel driven by a tangentially imposed electric field and/or pressure gradient was analytically studied. The surface charge densities (or relative surface potentials) of the slit walls can be arbitrary and unequal. Explicit formulas for the fluid velocity profile, average electroosmotic velocity, and average electric conductivity in the slit were obtained. Our results of salt-free solutions in a slit will be compared with those of salt-containing solutions and in a circular tube.

2. Analysis

We consider the electrokinetic flow of a salt-free solution in a slit microchannel or nanochannel between two large parallel plane walls at separation $2h$ with constant surface charge densities σ (at $y = h$) and $\beta\sigma$ (at $y = -h$) caused by a constant pressure gradient and a constant electric field, both are tangentially applied, as shown in Fig. 1. The surface charges of the slit walls and counterions (sole ionic species) in the solution are generated by a dissociation reaction taking place at the ionogenic groups uniformly distributed over each wall and $0 \le \beta \le 1$ is set without loss of generality. Evidently, the concentration of the counterions is a function of the lateral coordinate y (normal to the walls) and does not vary with the axial coordinate z (in the direction of fluid flow). Note that $\sigma = 2hZen_{av}/(1+\beta)$ due to the electric neutrality, where e is the elementary charge, $-Z$ is the valence of the counterions, and n_{av} is the average counterionic concentration in the salt-free solution in the slit.

2.1. Electric potential

The profiles of the equilibrium electric potential $\psi(y)$ and counterionic concentration $n(y)$ on a cross section of the slit needed to determine the fluid velocity distribution of the electrokinetic flow are governed by Poisson's equation,

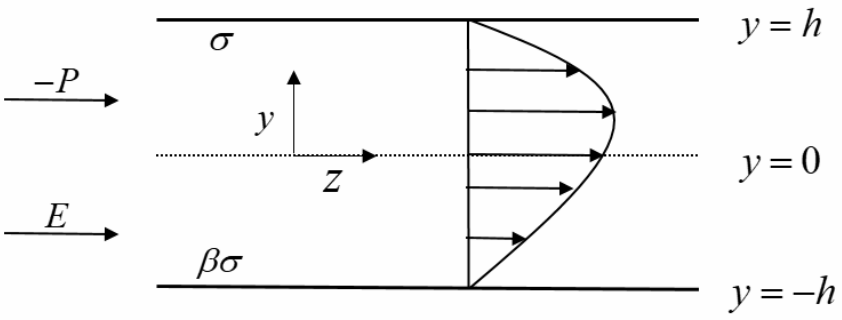

Fig. 1. Geometrical sketch for the electrokinetic flow in a charged slit.

$$\frac{\mathrm{d}^2\psi}{\mathrm{d}y^2} = \frac{1}{\varepsilon} Zen(y), \tag{1}$$

where ε is the dielectric permittivity of the fluid. The Boltzmann equation also provides a relation between the profiles $\psi(y)$ and $n(y)$,

$$n(y) = n(0)\mathrm{e}^{\bar{\psi}}, \tag{2}$$

where $\bar{\psi}(y) = Ze\psi / kT$, with k and T being the Boltzmann constant and absolute temperature, respectively, is the dimensionless potential profile, $y = 0$ denotes the location of the midplane between the slit walls, and $\psi(0) = 0$ is set in this equation.

Substituting Eq. (2) into Eq. (1), one obtains the Poisson-Boltzmann equation,

$$\frac{\mathrm{d}^2\bar{\psi}}{\mathrm{d}y^2} = \kappa^2 \mathrm{e}^{\bar{\psi}}, \tag{3}$$

where $\kappa = Ze[n(0) / \varepsilon kT]^{1/2}$ is the Debye screening parameter. The boundary conditions for $\bar{\psi}$ at the slit walls are

$$y = h: \quad \frac{\mathrm{d}\bar{\psi}}{\mathrm{d}y} = \frac{\bar{\sigma}}{h}, \tag{4}$$

$$y = -h: \quad \frac{\mathrm{d}\bar{\psi}}{\mathrm{d}y} = -\beta\frac{\bar{\sigma}}{h}, \tag{5}$$

where $\bar{\sigma} = hZe\sigma / \varepsilon kT = 2(\kappa h)^2 n_{\mathrm{av}} / (1+\beta)n(0)$ is the dimensionless surface charge density and Eqs. (4) and (5) are the Gauss conditions. Note that the dimensionless electrokinetic parameter κh depends upon $\bar{\sigma}$ (which is positive, since σ and Z have the same sign) and β (the square of κh is equivalent to the dimensionless average surface charge density of the slit walls), unlike the case of salt-containing solutions where κh is essentially independent of $\bar{\sigma}$ and β. Also, the ratio $n_{\mathrm{av}} / n(0)$ can be determined in terms of $\bar{\sigma}$ and β from an integration of $n(y)$ with respect to y in the whole range using Eq. (2).

An analytical solution to Eqs. (3)-(5) is [23]

$$\bar{\psi}(y) = \bar{\psi}_{\mathrm{m}} + \ln\sec^2[\frac{\lambda}{h}(y - y_{\mathrm{m}})], \tag{6}$$

where $\lambda = \kappa h \exp(\bar{\psi}_{\mathrm{m}} / 2) / \sqrt{2}$ is an integration constant, $\bar{\psi}_{\mathrm{m}} = \bar{\psi}(y_{\mathrm{m}}) \le 0$ is the minimum of the dimensionless potential profile $\bar{\psi}(y)$, and $-h \le y_{\mathrm{m}} \le 0$ with $0 \le \beta \le 1$. For specified values of $\bar{\sigma}$ and β, the values of λ and y_{m} / h can be obtained numerically from the simultaneous algebraic equations resulting from the substitution of Eq. (6) into Eqs. (4) and (5),

$$2\lambda \tan\theta_+ = \bar{\sigma}, \tag{7}$$

$$2\lambda \tan\theta_- = \beta\bar{\sigma}, \tag{8}$$

where

$$\theta_\pm = \lambda(1 \mp \frac{y_{\mathrm{m}}}{h}). \tag{9}$$

With the solution of $\bar{\psi}(y)$ in Eq. (6), the dimensionless concentration distribution $n(y) / n(0)$ of the counterions can be determined using Eq. (2). Substituting $\bar{\psi}(0) = 0$ into Eq. (6), one obtains

$$\kappa h = \sqrt{2}\lambda \sec(\lambda \frac{y_{\mathrm{m}}}{h}), \tag{10}$$

which again implies that κh depends on $\bar{\sigma}$ and β.

From Eq. (6), the relative surface potentials of the two slit walls can be expressed individually as

$$\zeta_\pm = \psi(\pm h) - \psi_{\mathrm{m}} = \frac{kT}{Ze} \ln\sec^2\theta_\pm, \tag{11}$$

and the dimensionless potentials $Ze\zeta_\pm / kT$ are positive functions of β and $\bar{\sigma}$ or κh increasing from zero at $\bar{\sigma} = \kappa h = 0$ with $|\zeta_-| \le |\zeta_+|$. Note that, for a given value of $\bar{\sigma}$, $Ze\zeta_+ / kT$ increases with a decrease in β, while $Ze\zeta_- / kT$ decreases with a decrease in β.

When $|\bar{\psi}|$ is less than the order of unity, the Debye-Hückel approximation applies and Eq. (3) can be linearized as

$$\frac{\mathrm{d}^2\bar{\psi}}{\mathrm{d}y^2} = \kappa^2(1 + \bar{\psi}). \tag{12}$$

The solution to Eqs. (12), (4), and (5) can be obtained explicitly as

$$\overline{\psi}(y) = -1 + \frac{\overline{\sigma}}{\kappa h}(\mathrm{e}^{4\kappa h} - 1)^{-1}[(\mathrm{e}^{2\kappa h} + \beta)\mathrm{e}^{\kappa(h+y)} + (1 + \mathrm{e}^{2\kappa h}\beta)\mathrm{e}^{\kappa(h-y)}]. \quad (13)$$

Both Eq. (6) and Eq. (13) satisfy the requirement of $\overline{\psi} = 0$ in the limiting case of $\overline{\sigma} = 0$.

For the special case of $\beta = 1$ (both walls of the slit are equally charged, $\psi(y)$ and $n(y)$ are symmetric about $y = 0$, and $y_m = \overline{\psi}_m = 0$), Eqs. (6)-(10) reduce to

$$\overline{\psi}(y) = \ln \sec^2(\lambda \frac{y}{h}), \quad (14)$$

$$\theta_+ = \theta_- = \lambda = \kappa h / \sqrt{2} < \pi / 2, \quad (15)$$

$$2\lambda \tan \lambda = \overline{\sigma}, \quad (16)$$

and Eq. (13) becomes

$$\overline{\psi}(y) = -1 + \frac{\overline{\sigma}}{\kappa h}\frac{\cosh(\kappa y)}{\sinh(\kappa h)}. \quad (17)$$

Both Eq. (14) and Eq. (17) indicate that $\overline{\psi} \geq 0$ (viz., ψ and σ have the same sign) everywhere, and Eq. (15) indicates that the two electric double layers (with the characteristic thickness κ^{-1}, which is large) in the slit containing a salt-free solution overlap noticeably with each other regardless of the finite value of $\overline{\sigma}$.

2.2. Fluid velocity

The velocity distribution $u(y)$ for the electrokinetic flow of a salt-free solution within a slit channel caused by the applied pressure gradient P and electric field E in the z direction is governed by the conservative equation of fluid momentum,

$$\eta \frac{\mathrm{d}^2 u}{\mathrm{d}y^2} = ZeEn(y) - P, \quad (18)$$

where η is the fluid viscosity and $Zen(y)$ is the local space charge density. The boundary conditions for u at the no-slip slit walls are

$$y = \pm h: \quad u = 0. \quad (19)$$

With the substitution of Eq. (1) for $n(y)$, Eqs. (18) and (19) can be analytically solved as

$$u = -\frac{\varepsilon E}{\eta}\{\psi(h) - \psi(y) - \frac{1}{2h}(h - y)[\psi(h) - \psi(-h)]\} + \frac{P}{2\eta}(h^2 - y^2), \quad (20)$$

where $\psi(y)$ was given by Eq. (6) or (13). For the special case of $\beta = 1$(the slit walls are equally charged), $u(y)$ is symmetric about $y = 0$.

The average fluid velocity over a cross section of the planar slit can be defined as

$$< u > = \frac{1}{2h}\int_{-h}^{h} u(y)\mathrm{d}y = L_{11}P + L_{12}E, \quad (21)$$

where L_{11} and L_{12} are two Onsager transport coefficients [27, 28]. The substitution of Eq. (20) into Eq. (21) leads to

$$L_{11} = \frac{h^2}{3\eta}, \quad (22)$$

$$L_{12} = -\frac{\varepsilon}{2\eta}[\psi(h) + \psi(-h) - \frac{1}{h}\int_{-h}^{h}\psi(y)\mathrm{d}y]. \quad (23)$$

Equation (20) with $P = 0$ gives the electroosmotic velocity distribution $u^{(e)}(y)$ in the slit and $<u^{(e)}> = L_{12}E$ is the average electroosmotic velocity.

When the Debye-Hückel approximation applies, $\overline{\psi}(y)$ is given by Eq. (13) and Eq. (23) can be analytically calculated to yield

$$L_{12} = -\frac{\varepsilon kT\overline{\sigma}(1+\beta)}{2Ze\eta\kappa h}(\frac{\mathrm{e}^{2\kappa h}+1}{\mathrm{e}^{2\kappa h}-1} - \frac{1}{\kappa h}). \quad (24)$$

2.3. Electric conductivity

The electric current density distribution in the charged slit filled with a salt-free solution in the direction of the electrokinetic flow is

$$i(y) = E\Lambda(y) - Zen(y)u(y), \quad (25)$$

where the local electric conductivity of the solution at rest is

$$\Lambda(y) = \frac{1}{kT} Z^2 e^2 D n(0) \mathrm{e}^{\overline{\psi}}, \tag{26}$$

and D is the diffusivity of the counterions.

The average electric current density over a cross section of the slit can be expressed as

$$< i > = L_{21} P + L_{22} E, \tag{27}$$

where L_{21} (equal to L_{12} in Eq. (21) from the Onsager reciprocity principle) and L_{22} are the other two transport coefficients [28, 29]. Substituting Eqs. (1) and (20) for $n(y)$ and $u(y)$, respectively, into Eqs. (25) and (27), we obtain the average electric conductivity in the absence of the applied pressure gradient as

$$L_{22} = < \Lambda > + \frac{\varepsilon^2}{2\eta h} \int_{-h}^{h} (\frac{\mathrm{d}\psi}{\mathrm{d}y})^2 \mathrm{d}y - \frac{\varepsilon^2}{4\eta h^2} [\psi(h) - \psi(-h)]^2 . \tag{28}$$

The substitution of Eqs. (6) and (26) into Eq. (28) results in

$$L_{22} = \Lambda(0) [\frac{\varepsilon}{\eta D} (\frac{kT}{Ze})^2 J_1 + J_2], \tag{29}$$

where

$$J_1 = \frac{1}{(\kappa h)^2} [2\lambda(\tan\theta_+ + \tan\theta_- - 2\lambda) - (\ln \frac{\sec\theta_+}{\sec\theta_-})^2], \tag{30}$$

representing the contribution from the electroosmosis, and

$$J_2 = \frac{< \Lambda >}{\Lambda(0)} = \frac{\mathrm{e}^{\overline{\psi}_\mathrm{m}}}{2\lambda} (\tan\theta_+ + \tan\theta_-) . \tag{31}$$

Evidently, both J_1 and J_2 are positive, and $L_{22} = \Lambda = 0$ if $\overline{\sigma} = 0$.

When the Debye-Hückel approximation applies, $\overline{\psi}(y)$ is given by Eq. (13) and Eqs. (30) and (31) reduce to

$$J_1 = \frac{-\mathrm{e}^{4\kappa h} \overline{\sigma}^2}{2(\mathrm{e}^{4\kappa h} - 1)^2 (\kappa h)^4} \{3(1-\beta)^2 + 4(1+\beta^2)(\kappa h)^2 - 4[(1-\beta)^2 - 2\beta(\kappa h)^2]\cosh(2\kappa h) + (1-\beta)^2 \cosh(4\kappa h) - \kappa h [4\beta \sinh(2\kappa h) + (1+\beta^2)\sinh(4\kappa h)]\}, \tag{32}$$

$$J_2 = \frac{\sinh(\kappa h)}{\kappa h} . \tag{33}$$

3. Results and discussion

3.1. Electric potential

In Figs. 2 and 3, the dimensionless equilibrium electric potential $\overline{\psi}$ in a charged planar slit filled with a salt-free solution given by Eqs. (6)-(9) is plotted versus the relative position y / h for some values of the dimensionless surface charge density $\overline{\sigma}$ and ratio of surface charge densities of the two walls β. For the case of $\beta = 1$ (the two slit walls are equally charged, $\psi(y)$ is symmetric about $y = 0$, and $\overline{\psi}_\mathrm{m} = 0$), as shown in Fig. 2, the value of $\overline{\psi}$ declines monotonically with a decrease in the magnitude of y / h from a positive value $Ze\zeta_\pm / kT$ (where $\zeta_- = \zeta_+$) at $y / h = \pm 1$ (the slit walls) to zero at $y / h = 0$ (the midplane between the slit walls) for a given value of $\overline{\sigma}$ and rises monotonically with an increase in $\overline{\sigma}$ (or κh or $Ze\zeta_\pm / kT$) from zero at $\overline{\sigma} = 0$ (or $\kappa h = 0$ or $Ze\zeta_\pm / kT = 0$) for a given value of y / h. This outcome reflects the fact that the counterionic concentration grows with an increase in the magnitude of y / h, which is more significant when the surface charge density of the walls is higher.

For any case of $0 \le \beta < 1$ (the slit walls are unequally charged), as shown in Fig. 3, the value of $\overline{\psi}$ first declines with a decrease in y / h from a

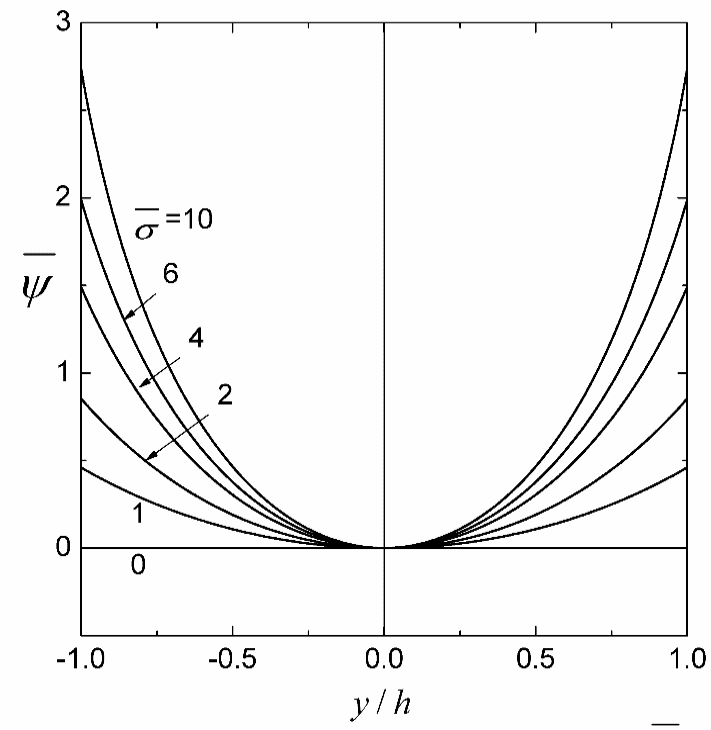

Fig. 2. The dimensionless electric potential $\overline{\psi}$ in a slit versus the relative coordinate y / h for the case of $\beta = 1$ with various values of $\overline{\sigma}$.

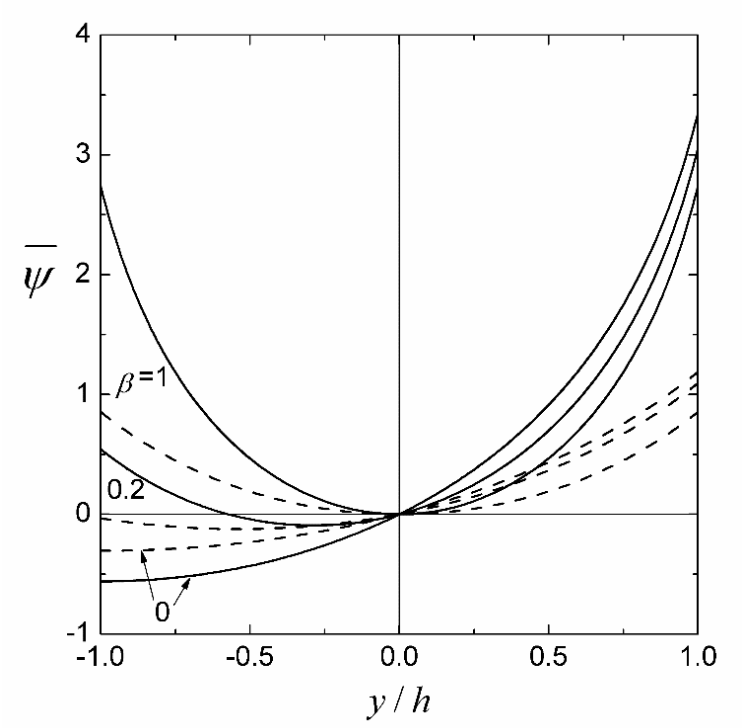

Fig. 3. The dimensionless electric potential $\overline{\psi}$ in a slit versus the relative coordinate y / h for the cases of $\overline{\sigma} = 10$ (solid curves) and $\overline{\sigma} = 2$ (dashed curves) with various values of β.

positive value at $y / h = 1$ (the higher-charged wall, to which most counterions are attracted due to the Coulomb force), becomes negative (where ψ and σ have opposite signs) as y / h is smaller than zero, reaches a minimum $\overline{\psi}_m$ at $y / h = y_m / h < 0$, and then rises with a further decrease in y / h till $y / h = -1$ (the lower-charged wall) for a constant value of $\overline{\sigma}$. The value of y_m / h drops with a decrease in β from zero at $\beta = 1$ to –1 at $\beta = 0$. The value of $\overline{\psi}$ at $y / h = -1$ can be positive (but no greater than that at $y / h = 1$) or negative, depending on the values of $\overline{\sigma}$ and β. For specified values of y / h and $\overline{\sigma}$, $\overline{\psi}$ rises with a decrease in β if $y / h > 0$ and declines with a decrease in β if $y / h > 0$. In general, the magnitude of $\overline{\psi}$ grows with an increase in $\overline{\sigma}$ from zero at $\overline{\sigma} = 0$ for fixed values of β and y / h (with exceptions as $y / h < 0$).

In Figs. 4 and 5, the dimensionless relative surface potentials $Ze\zeta_+ / kT$ and $Ze\zeta_- / kT$ of the higher-charged and lower-charged walls, respectively, calculated from Eq. (11) using both Eqs. (6)-(9) for the exact solution and Eq. (13) for the Debye-Hückel approximate solution of the electric potential profile $\overline{\psi}(y)$ in a slit filled with a salt-free solution are plotted versus the dimensionless surface charge density $\overline{\sigma}$ for several values of the surface charge density ratio β. As expected, both $Ze\zeta_+ / kT$ and $Ze\zeta_- / kT$ are increasing functions of $\overline{\sigma}$ (or κh) from zero at $\overline{\sigma} = 0$ for a given value of β, and $Ze\zeta_- / kT$ declines with a decrease in β to zero at $\beta = 0$, while $Ze\zeta_+ / kT$ rises with a decrease in β, for a given value of $\overline{\sigma}$. When $\overline{\sigma} \le 2$, $Ze\zeta_- / kT$ and $Ze\zeta_+ / kT$ are almost proportional to $\overline{\sigma}$ and their results obtained using Eq. (13) are in good agreement with those using Eqs. (6)-(9). When $\overline{\sigma} > 2$, the growths of $Ze\zeta_+ / kT$ and $Ze\zeta_- / kT$ with increasing $\overline{\sigma}$ are noticeably suppressed due to strong electrostatic screening with counterion condensation near the slit walls. For a salt-free solution in a circular tube with a fixed surface charge density [26], its relative surface potential is smaller than our result in a corresponding slit with $\beta = 1$ provided that the slit thickness $2h$ equals the tube diameter.

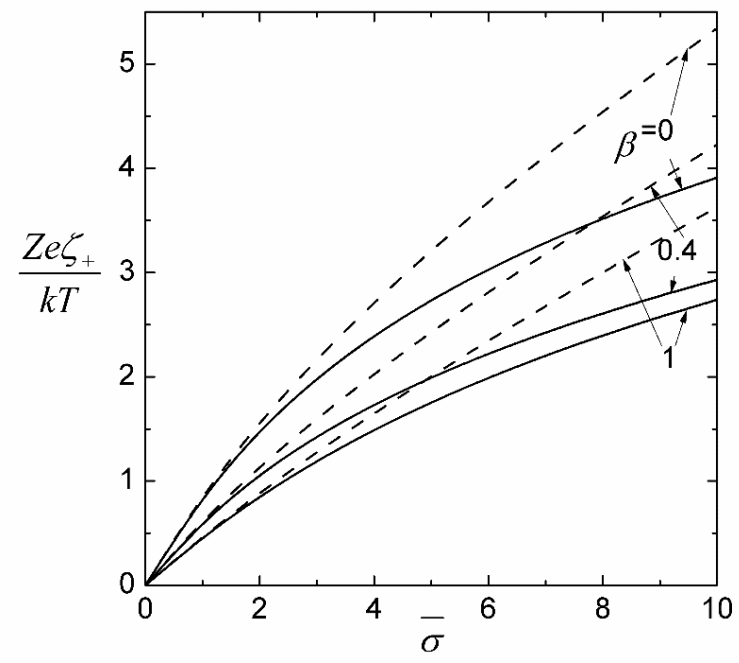

Fig. 4. The dimensionless relative surface potential $Ze\zeta_+ / kT$ in a slit versus the dimensionless surface charge density $\overline{\sigma}$ for several values of β. Solid lines represent the solution (6) of the full Poisson-Boltzmann equation; dashed lines the solution (13) of the linearized equation.

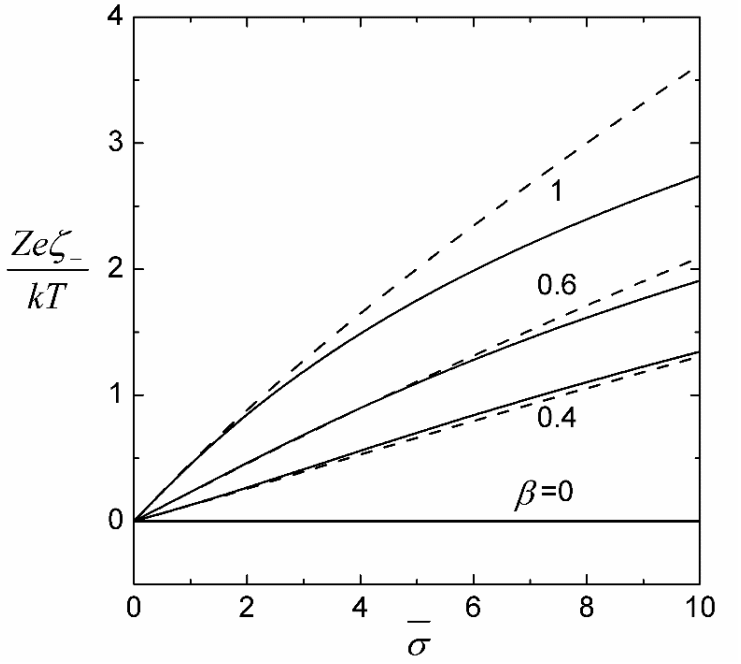

Fig. 5. The dimensionless relative surface potential $Ze\zeta_- / kT$ in a slit versus the dimensionless surface charge density $\bar{\sigma}$ for various values of β. Solid lines represent the solution (6) of the full Poisson-Boltzmann equation; dashed lines the solution (13) of the linearized equation.

3.2. Electroosmotic velocity

The results of the normalized electroosmotic velocity $-\eta u^{(e)} / \varepsilon\zeta_+ E$ (which is positive) of a salt-free fluid in a charged slit calculated from Eq. (20) with $\psi(y)$ given by Eqs. (6)-(9) and $P = 0$ are plotted versus the relative coordinate y / h in Figs. 6 and 7 for several values of the dimensionless surface charge density $\bar{\sigma}$ and ratio of surface charge densities of the two walls β. For the case of $\beta = 1$ (the two walls are equally charged and $u^{(e)}(y)$ is symmetric about $y = 0$), as shown in Fig. 6, this fluid velocity upsurges monotonically with a decrease in the magnitude of y / h from zero at $y / h = \pm 1$ (the no-slip walls) to unity at $y / h = 0$ (the midplane) for any given value of $\bar{\sigma}$ (or κh or $Ze\zeta_\pm / kT$). This outcome deviates from the electroosmosis of a corresponding salt-containing solution (in which κh is essentially independent of $\bar{\sigma}$), where $-\eta u^{(e)} / \varepsilon\zeta_\pm E = 1$ (the Helmholtz-Smoluchowski result) at $y / h = 0$ occurs only for the case of $\kappa h \to \infty$ [1, 3]. On the other hand, $-\eta u^{(e)} / \varepsilon\zeta_\pm E$ rises monotonically with an increase in $\bar{\sigma}$ for a given value of y / h, like that appearing in a salt-containing solution and consistent with experimental results of a salt-free solution in a circular tube [20]. Note that $-\eta u^{(e)} / \varepsilon\zeta_\pm E$ is finite (with $\zeta_\pm = 0$ and $u^{(e)} = 0$) in the limit of $\bar{\sigma} = 0$.

For any case of $0 \le \beta < 1$ (the walls are unequally charged), as shown in Fig. 7, the value of $-\eta u^{(e)} / \varepsilon\zeta_+ E$ first upsurges with a decrease in y / h from zero at $y / h = 1$ (the higher-charged wall), reaches a maximum at $y / h = y_M / h > 0$, and then decays with a further decrease in y / h back to zero at $y / h = -1$ (the lower-charged wall) for a given value of $\bar{\sigma}$. The value of y_M / h rises with a decrease in β from zero at $\beta = 1$ for a given value of $\bar{\sigma}$ and with an increase in $\bar{\sigma}$ from zero at $\bar{\sigma} = 0$ for a given value of β. Again, $-\eta u^{(e)} / \varepsilon\zeta_+ E$ increases with an increase in $\bar{\sigma}$ from zero at $\bar{\sigma} = 0$ for constant values of y / h and β. For fixed values of y / h and $\bar{\sigma}$, $-\eta u^{(e)} / \varepsilon\zeta_+ E$ declines with a decrease in β since less counterions are involved in their interaction with the applied electric field to produce the electroosmotic flow.

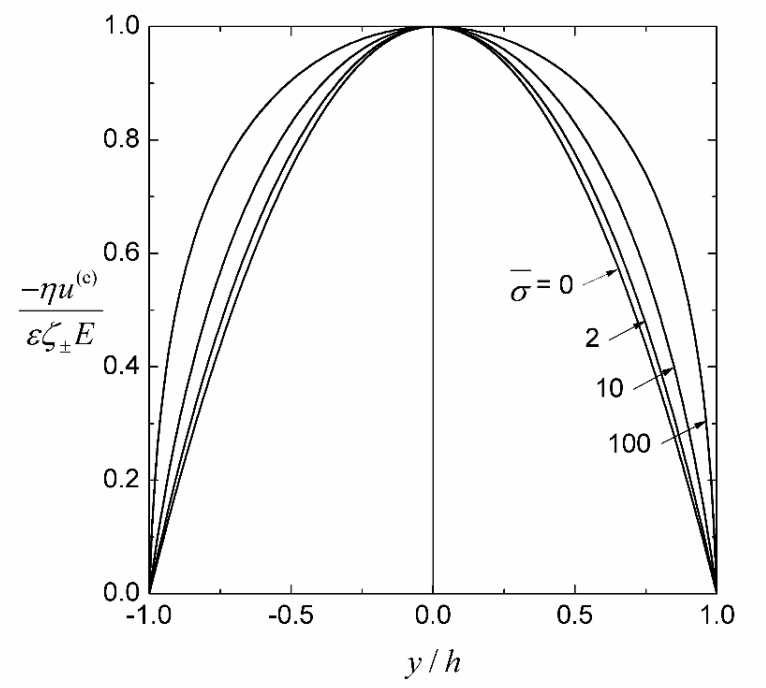

Fig. 6. The normalized electroosmotic velocity $-\eta u^{(e)} / \varepsilon\zeta_{\pm}E$ in a slit versus the relative coordinate y / h for the case of β = 1 with several values of $\overline{\sigma}$.

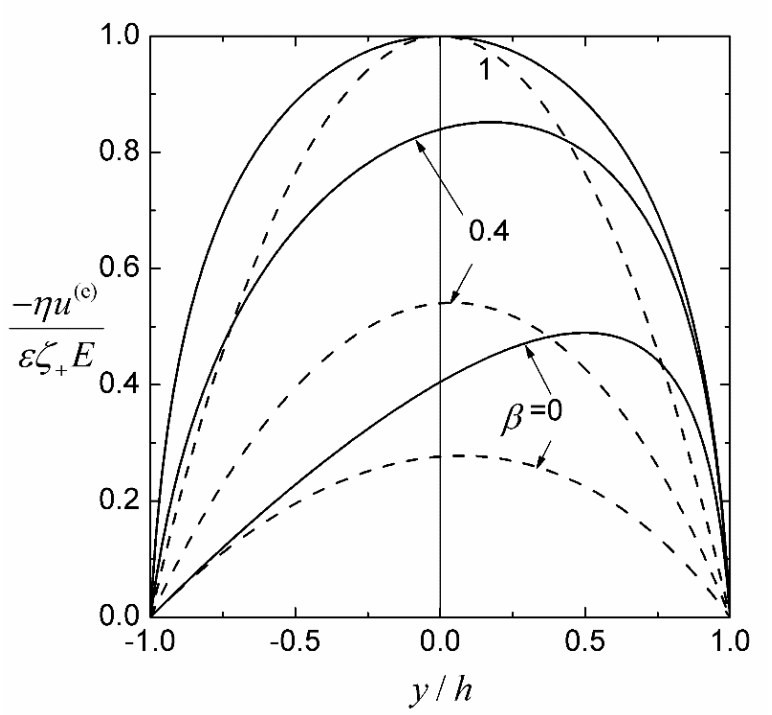

Fig. 7. The normalized electroosmotic velocity $-\eta u^{(e)} / \varepsilon\zeta_{+}E$ in a slit versus the relative coordinate y / h for the cases of $\overline{\sigma} = 50$ (solid curves) and $\overline{\sigma} = 1$ (dashed curves) with various values of β.

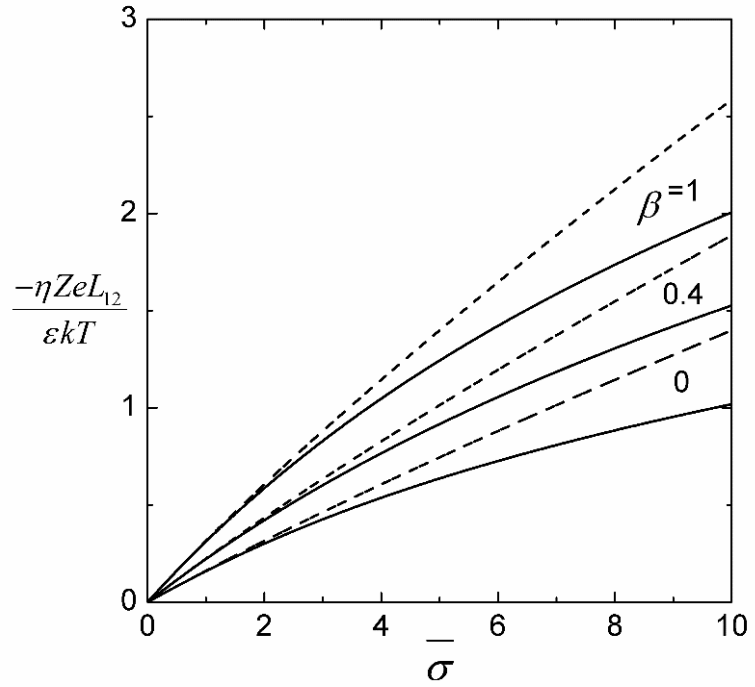

Fig. 8. The dimensionless average electroosmotic velocity $-\eta ZeL_{12}/\varepsilon kT$ in a slit versus the dimensionless surface charge density $\bar{\sigma}$ for several values of β. The solid and dashed curves represent results calculated using Eq. (23) with Eq. (6) and Eq. (24), respectively.

In Fig. 8, the dimensionless average electroosmotic velocity $-\eta ZeL_{12}/\varepsilon kT$ of a salt-free fluid in a charged slit calculated using the exact solution in Eqs. (6)-(9) and (23) as well as the approximate solution in Eq. (24) is plotted versus $\bar{\sigma}$ for several values of β. Like the dimensionless relative surface potentials $Ze\zeta_{\pm}/kT$ shown in Figs. 4 and 5, the agreement of the approximate and exact solutions of $-\eta ZeL_{12}/\varepsilon kT$ are good as $\bar{\sigma} \le 2$. Also like the normalized electroosmotic velocity profile $-\eta u^{(e)}/\varepsilon\zeta_{+}E$, this average velocity rises monotonically with an increase in $\bar{\sigma}$ (because more counterions are involved with the applied electric field to yield the electroosmotic flow) and drops with a decrease in β, keeping the other parameter unchanged. Again, $-\eta ZeL_{12}/\varepsilon kT$ is approximately proportional to $\bar{\sigma}$ as $\bar{\sigma} \le 2$ and its increase with $\bar{\sigma}$ is substantially suppressed due to the counterion condensation effect as $\bar{\sigma} > 2$. For a salt-free solution in a circular tube with a fixed surface charge density [26], its average electroosmotic velocity is smaller than our result in a corresponding slit with β = 1 and thickness 2h equal to the tube diameter.

3.3. Electric conductivity

The dimensionless electric conductivity $\eta(hZe/\varepsilon kT)^2(L_{22} - <\Lambda>)$ $[=(\kappa h)^2 J_1]$ brought by the electroosmotic flow in the charged slit filled with a salt-free solution is plotted versus the dimensionless surface charge density $\bar{\sigma}$ in Fig. 9 for various values of the ratio of surface charge densities of the two walls β calculated from the exact solution in Eq. (30) and approximate solution in Eq. (32). Analogous to the dimensionless relative surface potentials $Ze\zeta_{\pm}/kT$ in Figs. 4 and 5 and average electroosmotic velocity $-\eta ZeL_{12}/\varepsilon kT$ in Fig. 8, this conductivity drops with a decrease in β for a given value of $\bar{\sigma}$, and the agreement of the approximate and exact solutions is good as $\bar{\sigma} \le 2$. Like the electroosmosis of a salt-free solution in a circular tube [26], this conductivity increases monotonically with an increase in $\bar{\sigma}$ without being suppressed by the effect of counterion condensation. The electric

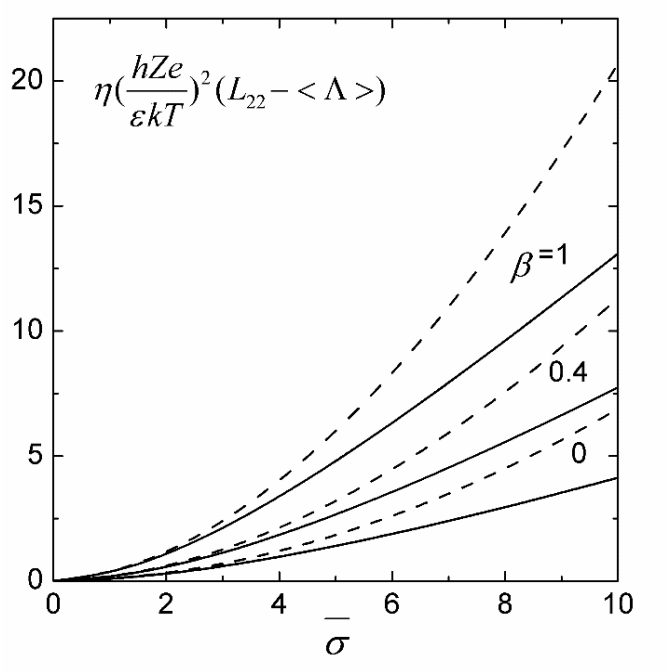

Fig. 9. The dimensionless electric conductivity $\eta(hZe/\varepsilon kT)^2(L_{22}-<\Lambda>)$ in a slit due to electroosmotic flow versus the dimensionless surface charge density $\bar{\sigma}$ for several values of β. The solid and dashed curves represent results calculated using Eqs. (30) and (32), respectively.

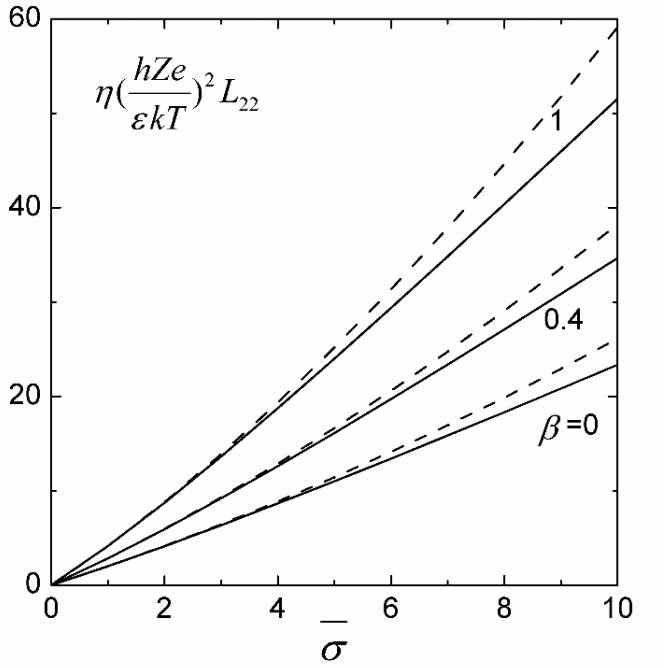

Fig. 10. The dimensionless overall electric conductivity $\eta(hZe/\varepsilon kT)^2 L_{22}$ of the aqueous solution of K^+ or Cl^- in a slit versus the dimensionless surface charge density $\bar{\sigma}$ for several values of β. The solid and dashed curves represent results calculated using Eq. (29) together with Eqs. (30) and (31) and Eqs. (32) and (33), respectively.

conductivity due to electroosmotic flow in the circular tube with a fixed surface charge density is greater than our result in a corresponding slit with $\beta = 1$.

The dimensionless overall electric conductivity $\eta(hZe/\varepsilon kT)^2 L_{22}$ (including the static contribution $< \Lambda >$) in a planar slit containing the aqueous solution of K^+ or Cl^- at room temperature (with $\varepsilon k^2 T^2/\eta De^2 = 0.26$ [29]) calculated using Eq. (29) plus Eqs. (30) and (31) for the exact solution and Eqs. (32) and (33) for the approximate solution of the coefficients J_1 and J_2 is plotted versus $\overline{\sigma}$ in Fig. 10 for several values of β. Again, the approximate solution agrees well with the exact solution as $\overline{\sigma} \le 2$. The value of $\eta(hZe/\varepsilon kT)^2 L_{22}$ is almost proportional to $\overline{\sigma}$ and declines with a decrease in β, keeping the other parameter unchanged. A comparison of Figs. 9 and 10 shows that $< \Lambda >$ contributes dominantly to the overall conductivity because the counterionic diffusivity is relatively high. When the value of $\overline{\sigma}$ (or $Ze\zeta_\pm / kT$ or κh) is small, the electroosmotic contribution to the overall conductivity is negligible for a salt-free solution, which differs from that for a salt containing solution in which $\overline{\sigma}$ and κh are independent of each other [1, 3]. The overall electric conductivity in the circular tube [26] with a fixed surface charge density is also greater than our result in a corresponding slit with $\beta = 1$.

4. Conclusions

An analytical study for the electrokinetic flow and attended electric conduction of a salt-free solution in a narrow slit channel between two parallel plane walls with constant surface charge densities σ and $\beta\sigma$, respectively, subjected to a pressure gradient and an electric field is presented. The electric potential and fluid velocity profiles are determined by solving the exact and linearized Poisson-Boltzmann equations and modified Navier-Stokes equation, respectively. Explicit formulas are obtained for the electroosmotic velocity and electric conductivity as functions of the dimensionless surface charge density $\overline{\sigma}$ and surface charge density ratio β of the slit walls. The dimensionless relative surface potentials $Ze\zeta_\pm / kT$, average electroosmotic velocity $-\eta ZeL_{12}/\varepsilon kT$, and average electric conductivity rise monotonically with an increase in $\overline{\sigma}$ (or κh, the ratio of the half thickness of the slit h to the Debye screening length κ^{-1}) for a given value of β. But, the rises of $Ze\zeta_\pm / kT$ and $-\eta ZeL_{12}/\varepsilon kT$ with increasing $\overline{\sigma}$ are suppressed noticeably when $\overline{\sigma}$ is high due to the counterion condensation effect. For a salt-free solution in a circular tube with a fixed surface charge density, its relative surface potential and average electroosmotic velocity are smaller but its average electric conductivity is greater than our results in a corresponding slit with $\beta = 1$ and half thickness h equal to the tube radius.

ACKNOWLEDGMENT

This work was supported by the Ministry of Science and Technology of Taiwan under Grant MOST110-2221-E-002-017-MY3.

CONFLICT OF INTEREST STATEMENT

The authors declare no conflict of interest.

REFERENCES

1. Burgreen, D. and Nakache, F. R. 1964, J. Phys. Chem., 68, 1084.
2. Keh, H. J. and Liu, Y. C. 1995, J. Colloid Interface Sci., 172, 222.
3. Keh, H. J. and Tseng, H. C. 2001, J. Colloid Interface Sci., 242, 450.
4. Kang, Y., Yang, C. and Huang, X. 2002, J. Colloid Interface Sci., 253, 285.
5. Keh, H. J. and Ding, J. M. 2003, J. Colloid Interface Sci., 263, 645.
6. Chang, C. C. and Wang, C.-Y. 2009, Phys. Fluids, 21, 042002.
7. Stone, H. A., Stroock, A. D. and Ajdari, A. 2004, Annu. Rev. Fluid Mech., 36, 381.
8. Yuan, Z., Garcia, A. L., Lopez, G. P. and Petsev, D. N. 2007, Electrophoresis, 28, 595.
9. Bandopadhyay, A. and Chakraborty, S. 2012, Appl. Phys. Lett., 101, 043905.
10. Poddar, A., Dhar, J. and Chakraborty, S. 2017, Phys. Rev. E, 96, 013114.
11. Tsao, H.-K. 1998, J. Phys. Chem. B, 102, 10243.
12. Ohshima, H. 2002, J. Colloid Interface Sci., 255, 202.
13. Lobaskin, V., Dünweg, B. and Holm, C. 2004, J. Phys.: Condens. Matter, 16, S4063.

14. Carrique, F., Ruiz-Reina, E., Arroyo, F. J. and Delgado, A. V. 2006, J. Phys. Chem. B, 110, 18313.
15. Lobaskin, V., Dünweg, B., Medebach, M., Palberg, T. and Holm, C. 2007, Phys. Rev. Lett., 98, 176105.
16. Carrique, F., Ruiz-Reina, E., Lechuga, L., Arroyo, F. J. and Delgado, A. V. 2013, Adv. Colloid Interface Sci., 201-202, 57.
17. Ohshima, H. 2018, Colloid Polymer Sci., 296, 1293.
18. Qiao, R. and Aluru, N. R. 2003, J. Chem. Phys., 118, 4692.
19. Ohshima, H. 2004, Colloids Surfaces B, 38, 139.
20. Chang, F.-M., Chang, Y.-W., Sheng, Y.-J. and Tsao, H.-K. 2010, Appl. Phys. Lett., 97, 164101.
21. Chang, S.-H. 2009, Biomicrofluidics, 3, 012802.
22. Chang, S.-H. 2010, Eur. J. Mech. B/Fluids, 29, 337.
23. Chang, S.-H. 2012, Eur. J. Mech. B/Fluids, 34, 85.
24. Bandopadhyay, A. and Chakraborty, S. 2013, Electrophoresis, 34, 2193.
25. Su, Y. W. and Keh, H. J. 2019, J. Phys. Chem. B, 123, 9724.
26. Luo, R. H. and Keh, H. J. 2020, Electrophoresis, 41, 1503.
27. Donath, E. and Voigt, A. 1986, J. Colloid Interface Sci., 109, 122.
28. Gonzalez-Tovar, E., Lozada-Cassou, M. and Olivares, W. 1991, J. Chem. Phys., 94, 2219.
29. van de Ven, T. G. M. 1989, Colloidal Hydrodynamics, Academic Press, London.